Vortex Sheet Modeling with Curved Higher-Order Panels

M. G. Nagati*
Wichita State University, Wichita, Kansas
and
J. D. Iversen† and J. M. Vogel‡
Iowa State University, Ames, Iowa

A method is presented for predicting the geometry of a vortex sheet trailing a lift-generating wing. It differs from other methods in that it uses a continuous vorticity distribution and curved panels rather than discrete vortex filaments or flat panels. Although the original intent was to apply cyclic iterations to the computed results, it was found that the results of the initial cycle were already in good agreement with the experiment.

Nomenclature

a = coefficients of bicubic patch (panel) polynomials
b = wing span
c = local chord
C_ℓ = local section lift coefficient
i = index for patch or node, streamwise
j = index for patch or node, spanwise
m = number of patches or nodes, streamwise
n = number of patches or nodes, spanwise
s = arc length
t = time elapsed
u = parameter for patches interpolant, streamwise
v = parameter for patches interpolant, spanwise
V = induced velocity
V_∞ = freestream velocity
x = position vector of point with coordinates x,y,z
x_u = tangent vector to a v = constant curve, $\partial x/\partial u$
x_v = tangent vector to a u = constant curve, $\partial x/\partial v$
γ = vorticity strength
Γ = circulation

Introduction

A GOOD prediction of the rollup of the vortex sheet in the vicinity of its generating aircraft is essential for predicting the aerodynamic response of surfaces exposed to its influence. Potential flow panel methods are currently used extensively for preliminary evaluations of aircraft configuration. Simplifying assumptions regarding the vortex sheet, such as the neglect of rollup and vertical and lateral displacements, lead to erroneous evaluations of various stability derivatives and tail loads except for the simplest conditions, thus incurring a serious but unnecessary limitation on their application. Examples of panel method evaluations requiring vortex sheet configuration predictions include the following:

1) Control Effectiveness and Stability Derivatives. Downwash and sidewash estimates are required for empennage sizing. The current approach of using empirical or semiempirical data is useful only when applied to conventional configurations geometrically similar to the ones used in obtaining these data. The theoretical part of the semiempirical data can be generalized only if simplified to the point where applicability is limited. Variations in spanwise lift distribution due to flaps, nacelles and/or struts, ailerons, flow separation, etc. are likely to affect downwash and hence empennage lift distributions. In both symmetric and sideslip conditions, the empennage load predictions can be truly generalized only when these induced effects are taken into consideration.

2) Canard Configurations. Trailing vorticity from the canard will modify the spanwise lift distribution of the following main wing. Thus the wing's induced drag and stall characteristics are modified in a manner that may be adverse to the configuration's handling qualities.

3) Trailing Vortex Hazard Studies. These methods require the precise determination of the position and strength of the vortex cores following rollup completion so that their interaction can be studied farther downstream, where viscous effects, vortex merging, and energy dissipation are important.[1-3]

Background

The present method is based upon earlier work in three areas of computational methods developed in the last two decades.

The Panel Method

This highly successful technique is valuable for its reliability and accuracy for the prediction of pressure distribution on complete configurations. Early work by Smith and Hess and Rubbert was later expanded to utilize higher-order singularity distributions.[4-6] As a result, the panel model became more accurate and less sensitive to panel density.[7] For the most part, flat panel approximations were still used. Hess reported his investigations on the use of curved panels using a bicubic interpolant.[8,9] The concept of distributed vorticity is used in the present work to avoid discrete vortex filaments, therefore reducing the model's sensitivity to numerical problems.

Vortex Sheet Rollup

The present study is not concerned with the far downstream effects of decay and merging, on which much research has been done. (A rather thorough survey was compiled by El-Ramly.[10]) The first effort to predict the shape of trailing vortex filaments was that of Westwater.[11] More recently, this method was improved, extended to swept wings, and computerized.[12-14] These techniques were extended in the present case to the use of distributed vorticity.

Parametric Bicubic Surface Geometry

To represent the gometry of the surface of discontinuity (the vortex sheet), an array of parametric bicubic patches is used so

Presented as Paper 86-1812 at the AIAA 4th Applied Aerodynamics Conference, San Diego, CA, June 16-18, 1986; received Aug. 19, 1986; revision received March 6, 1987.

*Associate Professor, Aeronautical Engineering. Senior Member AIAA.
†Professor, Aerospace Engineering. Associate Fellow AIAA.
‡Associate Professor, Aerospace Engineering. Member AIAA.

that the surface is mathematically continuous to the second derivative. This technology is widely used in aircraft and automobile CAD/CAM techniques. The model used here is that of Ferguson.[15]

Description of the Method

Given a generating wing with a known lift distribution, the bound vorticity can be calculated by the application of the Kutta-Joukowski theorem of vortex lift:

$$L(y) = \rho V_\infty \Gamma(y)$$

The spanwise variation in $\Gamma(y)$ results in streamwise trailing vorticity. Three streamwise regions are defined for the free sheet:

1) The region of concern, where accurate estimates of induced velocities are needed.

2) The region where rollup affects region 1, both upstream and downstream.

3) The region extending far enough downstream to simulate the remainder of the semi-infinite vortex sheet. It is extended to such distance beyond which vorticity (with or without rollup) has negligible effects in regions 1 and 2.

The Geometric Model

The free sheet is represented geometrically by a rectangular array of parametric bicubic patches, m streamwise by n spanwise (Fig. 1). The distribution of patches is denser near the tip or in other areas of large changes in lift. This improves the accuracy of the interpolation for both the position and the magnitude of the vorticity, since these are places where large induced velocities will exist. A higher density is also desired near the trailing edge of the wing, where initial variations in shape are critical in determining the final shape of the vortex sheet.

Initially, the sheet is a flat extension of the trailing edge in the direction of the relative wind, the bicubic patches degenerating to bilinear form. After the first application of induced displacement, the sheet is no longer flat. The grid of nodes forming the corners of each patch is updated for each cycle, thus redefining the sheet geometry. Points interior to these patches are obtained by interpolation:

$$\boldsymbol{x} \equiv (x,y,z) = \sum_{k=0}^{3} \sum_{\ell=0}^{3} \boldsymbol{a}^i_{k\ell} u^k v^\ell \qquad (1)$$

$$0 \le u, \qquad v \le 1$$

where u and v are the parameters (Fig. 2) and $a_{k\ell}$ are sixteen vector coefficients. Each element of an $\boldsymbol{a}$ vector corresponds to one of the elements (coordinates) of the geometric position vector $\boldsymbol{x}$ of the point on the sheet on which the jump in the velocity potential function occurs.

Assuming that for a given cycle the position vectors at the nodes are known, additional data at these nodes are required for the evaluation of the $\boldsymbol{a}$ vectors. The parametric bicubic patches used here are of the Ferguson type.[13] These data are tangent vectors. Twist vectors are neglected. C^2 (i.e., second-derivative) continuity is required across the common edges of adjacent patches. This fact enables the writing of enough linear equations to solve for the tangent vectors x_u and x_v if they are known in the normal parametric direction at the sheet surface boundary.[15] This is done as follows:

1) For symmetric loading, only half the sheet is computed. Due to symmetry, the tangent vectors $\boldsymbol{x}_v$ are simply normal to the plane of symmetry.

2) The far downstream portion of the boundary is the intersection of the vortex sheet with the Trefftz plane (Fig. 1). There, the tangent vectors $\boldsymbol{x}_u$ are considered normal to that plane.

3) At the trailing edge of the generating wing, the tangent vectors $\boldsymbol{x}_u$ are updated with every cycle (even though little change occurs there) and are parallel to the velocity of the air particle leaving the trailing edge:

$$\boldsymbol{V}_\infty + \boldsymbol{V}_i$$

where $\boldsymbol{V}_\infty$ is the freestream wind velocity and $\boldsymbol{V}_i$ is the induced velocity at the node in question.

4) The boundary portion trailing from the wing tip is more involved. The tangent vector must be obtained by computing a velocity gradient component along a spanwise curve.

Let the point A on the boundary (Fig. 3) have the position vector $\boldsymbol{x}$. A point just inboard of it (B) has the position $\boldsymbol{x} + \mathrm{d}\boldsymbol{x}$ where $\mathrm{d}\boldsymbol{x} = \boldsymbol{x}_v \mathrm{d}v$ and $\mathrm{d}v$ is the parametric distance between the two points A and B in Fig. 3. The difference in induced velocity at these two points is

$$\mathrm{d}\boldsymbol{V} = \frac{\partial \boldsymbol{V}}{\partial v} \mathrm{d}v \qquad (2)$$

After a time t has elapsed, the new location of these two points is A' and B' separated by

$$\mathrm{d}\boldsymbol{x}' = (\mathrm{d}y',\ \mathrm{d}z') \qquad (3)$$

where

$$\mathrm{d}y' = \mathrm{d}y + \mathrm{d}V_y t$$

$$\mathrm{d}z' = \mathrm{d}z + \mathrm{d}V_z t$$

Thus the required tangent vector is

$$\boldsymbol{x}'_v = v\left(\boldsymbol{x}_v + \frac{\partial \boldsymbol{V}}{\partial v} t\right) \qquad (4)$$

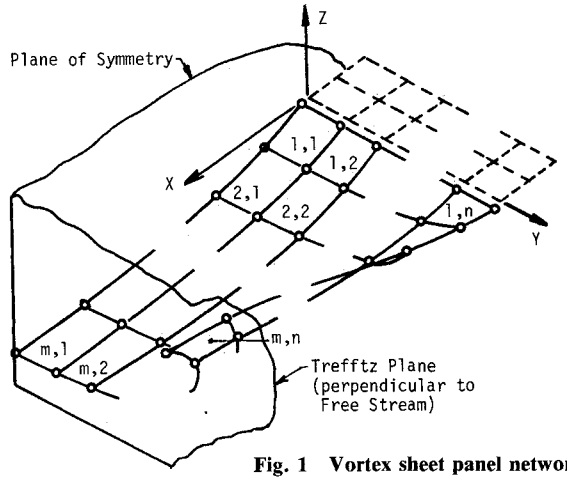

Fig. 1 Vortex sheet panel network.

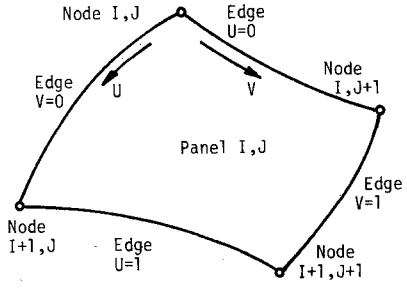

Fig. 2 Panel nomenclature.

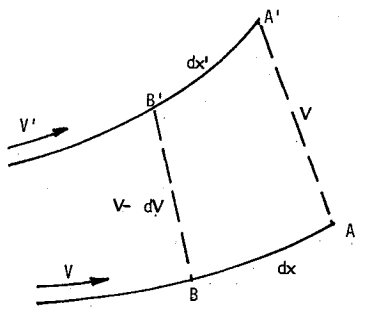

Fig. 3 Tangent vector at the tip edge.

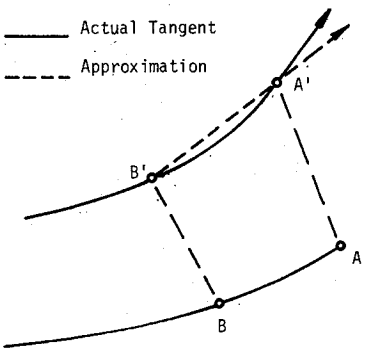

Fig. 4 Tangent vector approximation.

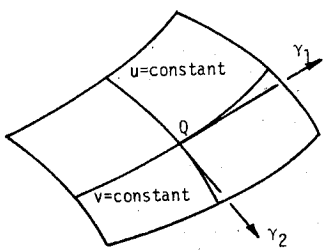

Fig. 5 Panel vorticity.

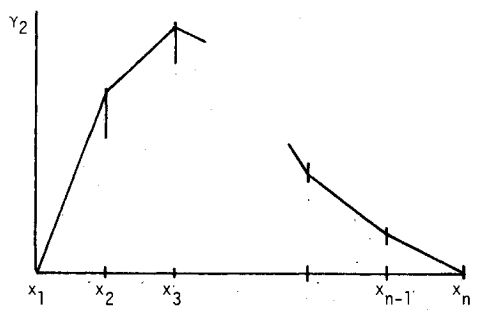

Fig. 6 Approximation of chordwise distribution of vorticity.

ν is a factor determined by smoothing to adjust the magnitude of the tangent vector, as will be discussed.

The computation of the velocity gradient is equivalent to the computation of the induced velocity at another point; thus a finite-difference δv is used instead of a differential dv. The results are nearly the same. Figure 4 depicts the approximate tangent vector.

The computation of the induced velocity is accomplished by a Gaussian quadrature, a numerical integration scheme that minimizes error. It is suitable for this computation because the integrand is evaluated away from singularities. However, for the tangent vector computation at the tip using either method, the interior point used to compute it is subjected to larger induced velocities (due to the vorticity lumped at the quadrature points) than is the tip itself. This is contrary to the physical nature of the problem. Other numerical quadrature schemes did not succeed because the distances involved in the integrand are raised to a negative power, leading to excessive roundoff errors. Double precision in the computation was not used because the computation time and storage requirements would have been excessive. To improve this estimate, a smoothing technique is applied to each spanwise curve at the streamwise station being processed.

Smoothing

In the smoothing scheme, the position vectors at all the nodes are assumed to be correct as are the tangent vector directions except at the tip. The design variables in the smoothing problem are 1) the tangent vector direction at the tip, and 2) a factor ν multiplying the initial estimate of the tangent vector for all nodes. The tangent vector magnitude is initially the neighboring chord length for the interior nodes and is defined by Eq. (4) at the tip. The objective function F is a weighted sum of two integrals over the length of the curve:

$$F = \int K^2 ds + w \int ds \tag{5}$$

K is the local curvature

$$\frac{x_v y_{vv} - y_v x_{vv}}{(x_v^2 + y_v^2)^{1.5}}$$

and

$$ds = (y_v^2 + z_v^2)^{0.5} dv$$

w is a weight factor selected by visually comparing the results. (The value used is 500 m^{-2}.)

The steepest descent method is used to minimize F. Conjugate gradient methods were not as successful. A small number of line searches (two or three) are required. Each line search is limited to 10 iterations because changes in F are small. The preceding integrals are evaluated using the trapezoidal rule.

As a result, the undesired reflex of the vortex sheet near the tip is removed, and the curves between the nodes become fuller. These effects greatly enhance the performance of the system at subsequent stream stations.

The Vorticity Model

In each of the sheet geometry patches, a parametric bilinear vorticity disribution is used:

$$\gamma(u,v) = U_{11}\gamma_{i,j} + U_{21}\gamma_{i+1,j} + U_{12}\gamma_{i,j+1} + U_{22}\gamma_{i+1,j+1} \tag{6}$$

where $\gamma_{i,j}$ is the magnitude of the vorticity at node i,j.

$$U_{11} = 1 - u - v + uv$$

$$U_{21} = u - uv$$

$$U_{12} = v - uv$$

$$U_{22} = uv$$

u and v are the same parameters as are used for geometry. Thus $\gamma(u,v)$ is the vorticity at the point $x(u,v)$. Doublet panels are equivalent to the vortex panels used here to represent the discontinuity in the potential function across the vortex sheet, and are used frequently because doublet strength is a scalar. Vorticity, on the other hand, is a vector lying in the vortex sheet and is preferred here since the bilinear distribution of vorticity is equivalent to biquadratic doublet strength. The truncation error order is not improved by using a biquadratic vorticity distribution, and its value is continuous across the patches, thus eliminating concentrated vorticity in the trailing sheet.

In the present method, the v = constant curves coincide with trailing filaments of infinitesimal strength in both the bound and free portions of the sheet, while the u = constant curves coincide with spanwise vorticity, which causes the lift. At any point on the sheet, the tangent vector (which is also tangent to a vortex filament) is $x_u(u,v)$ or $x_v(u,v)$ (Fig. 5).

Let γ_1 be the trailing vorticity strength and γ_2 that of the spanwise vorticity. Then the induced velocity at a point P (whose position vector is ξ) composed of V_1 and V_2 is

$$V_1^{i,j} = \int_0^1 \int_0^1 \frac{\gamma_1(u,v)}{4\pi} \frac{x_u \times (\xi - x)}{|x_u| \cdot |\xi - x|^3} J\,du\,dv$$

$$V_2^{i,j} = \int_0^1 \int_0^1 \frac{\gamma_2(u,v)}{4\pi} \frac{x_v \times (\xi - x)}{|x_v| \cdot |\xi - x|^3} J\,du\,dv$$

where

$$J = |x_u \times x_v|$$

Thus

$$V^{i,j} = V_1^{i,j} + V_2^{i,j} \tag{7}$$

For all the panels,

$$V = \sum_{i=1}^{m} \sum_{j=1}^{n} V^{i,j} \tag{8}$$

To compute the nodal vorticity using the wing spanwise and chordwise lift distribution, the Kutta-Joukowsky theorem and Helmholtz' first vorticity theorem are used. The lift coefficient C_ℓ, chord c, and circulation Γ are all functions of the spanwise distance y.

$$C_\ell = C_\ell(y) \tag{9a}$$

$$c = c(y) \tag{9b}$$

$$\Gamma(y) = \frac{1}{2} V_\infty c C_\ell \tag{9c}$$

Between two stations at y_j and y_{j+1}, γ_1 is linearly approximated by

$$\gamma_1(y) = \frac{(\gamma_1)_{j+1} - (\gamma_1)_j}{y_{j+1} - y_j}(y - y_j) + (\gamma_1)_j \tag{10}$$

The change in circulation is

$$\Gamma_{j+1} - \Gamma_j = \int_{y_j}^{y_{j+1}} \gamma_1 \, dy$$

$$= \frac{y_{i+1} - y_i}{2}[(\gamma_1)_{j+1} + (\gamma_1)_j] \tag{11}$$

Γ_j is also distributed linearly in the chordwise direction so that

$$\Gamma_j = \int_0^{C_j} \gamma_2 \, dx \tag{12}$$

where

$$\gamma_2(x) = \frac{(\gamma_2)_{i+1} - (\gamma_2)_i}{x_{i+1} - x_i}(x - x_i) + (\gamma_2)_i$$

as shown in Fig. 6. Thus (by trapezoidal rule integration)

$$\Gamma_j = \sum_{i=1}^{m} \frac{x_{i+1} - x_i}{2}[(\gamma_2)_{i+1} + (\gamma_2)_i] \tag{13}$$

If the ratio of the $(\gamma_2)_i$ values is known, then their values can be obtained. This ratio is obtained from the chordwise lift distribution. These relations are sufficient when applied at each station j to compute the vorticity at all the nodes of the sheet.

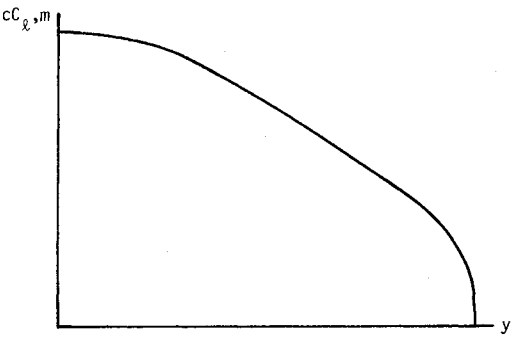

Fig. 7 Approximation of circular motion.

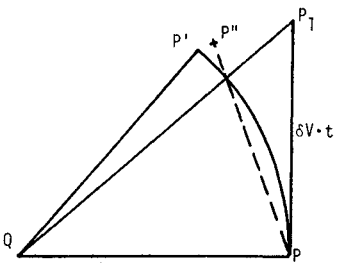

Fig. 8 Test wing load distribution.

The Computation Scheme

To obtain the rolled-up sheet configuration, the following scheme is performed:

1) The initial geometry consists of a grid of nodes (or an array of panels) for the bound portion of the sheet and another for the free portion as described in the geometric model. The free portion uses a set of spanwise curves (station i, $i = 1, 2, \ldots, m$) parallel to the wing trailing edge. Each curve i has the same number of nodes n. Node j in each curve has the same coordinates $y_{i,j}$, $z_{i,j}$. The x coordinate is such that $x_{i+1,j} - x_{i,j}$ is constant for all j.

2) Compute the nodal vorticities γ_1 and γ_2 as described in the vorticity model.

3) Compute the induced velocities due to the entire sheet at the nodes for station $i = 1$ (the trailing edge). Use these to compute the tangent vectors at station 1. Set $i = 2$.

4) Repeat while i is within regions 1 and 2:

a) Compute the induced velocities at the nodes for stations $1,2,\ldots,i$. The time lapse is

$$t_i = (x_i - x_{i-1})/V_\infty$$

The displacements of the nodes $x'_{i,j}$, $j = 1,2,\ldots,n$ are

$$x'_{i,j} = \frac{1}{2} t_i (V_{i,j} + V_{i-1,j})$$

The new position vectors for nodes i,j are then

$$x_{i,j} + x'_{i,j}$$

b) Compute the tangent vector x_v at node (i,n) as explained in the geometry modeling section.

c) Set $y_{k,j}$ equal to $y_{i,j}$, $z_{k,j}$ equal to $z_{i,j}$ and $x_{v(k,n)}$ equal to $x_{v(i,n)}$ for $k = i+1, i+2, \ldots, m$.

d) Next i.

The displacements of the nodes take place in curved paths. Because these paths are approximated with straight lines, the stations have to be very closely spaced. An approximation of the circular displacement is shown in Fig. 7. Point Q is on the vortex sheet and point P is a field point. An increment in the induced velocity δV due to the elemental vorticity at Q leads to a displacement $\delta V \cdot t$. P_1 is the result of linear displacement. P_2 is obtained by shortening QP_1 by the ratio QP/QP_1. Then PP_2 is stretched by the ratio PP_1/PP_2 to obtain P''. P'' is the approximation of the true position P'.

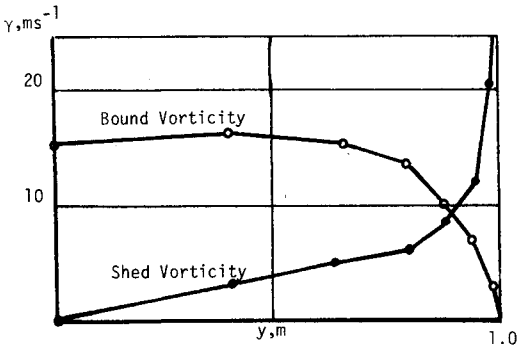

Fig. 9 Nodal vorticity at trailing edge.

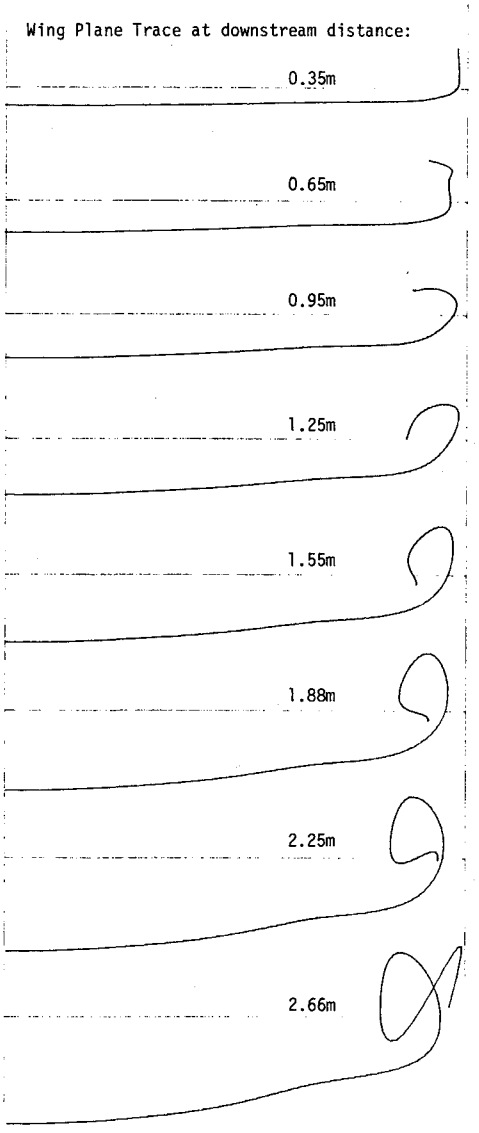

Fig. 10 Vortex sheet sections—no smoothing.

Results and Discussion

Tests were performed in the Boeing Research Wind Tunnel in Seattle on a half-span (1,016-mm) wing with a root chord of 406.4 mm, a taper ratio of one-half, and a straight unswept trailing edge.[16] It had a twist from zero at the root to −4 deg at the tip and no dihedral. The span load distribution is given in Fig. 8. The flow visualization was obtained at a station 2.5 m downstream. The wing and trailing vorticities are plotted in Fig. 9. This result was used for comparison with the computational method described in this paper. The streamwise stations used in the computation are at 0.05, 0.35, 0.65, 0.05, 1.25, 1.55, 1.88, 2.25, 2.66, 3.1, 3.7, 4.5, and 5.5 m from the trailing edge. The first nine are representative of regions 1 and 2; the others were not updated. The first station is at 0.05 rather than zero to avoid close proximity to the bound vorticity. Downwash angles thus calculated are more consistent with theory.

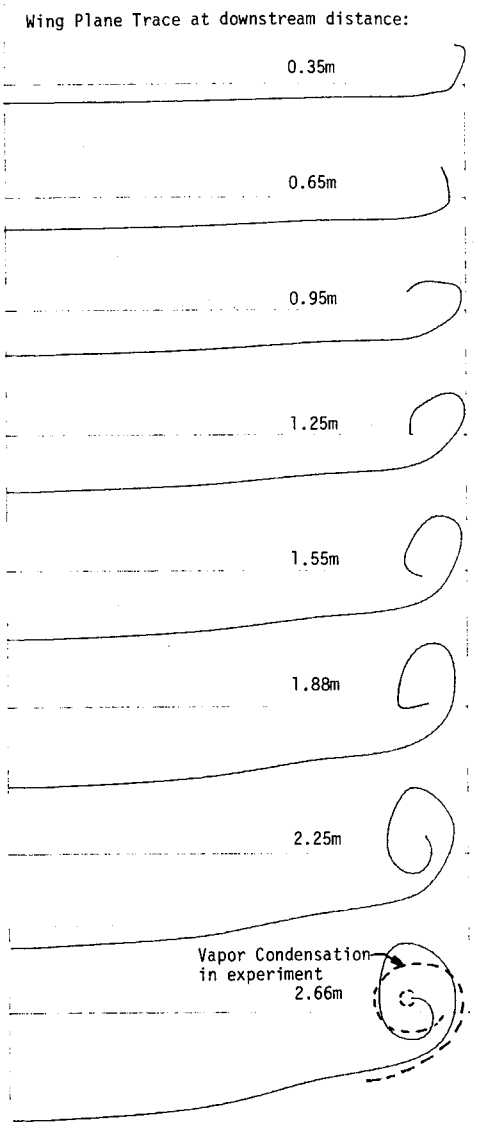

Fig. 11 Vortex sheet sections—with smoothing.

To illustrate the effect of smoothing, the computed vortex sheet shapes before smoothing was applied are plotted in Fig. 10. Some irregularities near the tip are evident due to the problems discussed earlier and include points of inflection as well as the vortex sheet crossing itself. Poor results in the early stages propagate downstream and cause increased error in the induced velocities and thus the sheet geometry.

In Fig. 11, these plots are shown after smoothing, which allows the tangent vector at the tip to vary. Intuitively, one would expect a smooth spiral without inflections, since the wing loading is monotonic from centerline to tip. The vortex sheet crossing itself is certainly not in agreement with the physics of fluid flow. Figure 11 shows that smoothing results in a significant improvement in the solution in the tip region, especially downstream from $x = 1.25$. The agreement with the experiment is as seen at station 2.66. (There is a small shift from the experimental station at 2.5, which was neglected.)

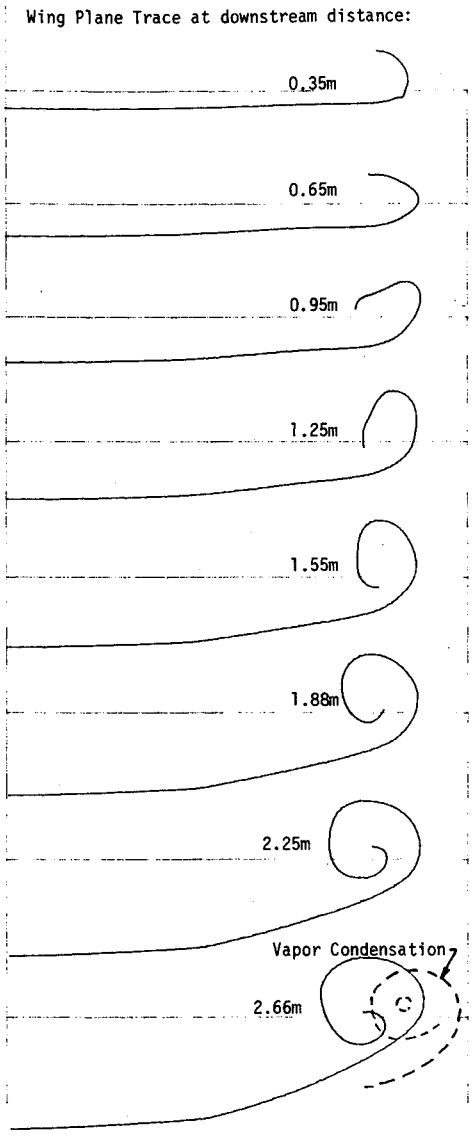

Fig. 12 Vortex sheet sections—with smoothing and Betz rule.

In order to compare with theory, the results were tested against Betz' first rule for the conservation of momentum.[17] The centroid of vorticity should remain at a constant span station. An error of approximately 8% occurs at the first station, remaining constant with downstream distance. An attempt to correct for that by shifting the curve nodes at each station to force the location of the centroid to match that at the trailing edge was performed.

Starting from the center node, each node is shifted by a fraction of the error equal to the ratio of the magnitude of the local to the total vorticities, dragging with it all the nodes outboard of it. Each time, the section curve is resmoothed until the tip is reached. This procedure is repeated for each station being processed before downstream stations are slaved to it, in conjunction with step 4c of the algorithm.

It was found that this correction for the momentum conservation error was necessary only at the first three stations. The first required two nodal displacements and the second only one. The correction results in a reduction in the smoothing effort in subsequent downstream sections. Although now the Betz rule is satisfied, the correlations with the test results are worse. It is believed that viscous and tip effects lead to this discrepancy (Fig. 12).

A second more complex loading condition simulating deflected part-span flaps was performed. Even though unsubstantiated by experiment, it shows the ability of the method to handle complex wing loadings at least within one span length downstream. At station 1.25, however, the vortex sheet crosses itself due to the curve fitting scheme used. Rather than requiring second-derivative continuity, a different condition must be imposed at the node with large vorticity, e.g., to treat it similar to the tip. This is not included in the present study.

Conclusions

The present method, because of the continuity in the vorticity distribution, is less sensitive to the positioning of nodes than methods using discrete vorticity. For downstream distances less than 1.25 times the wing half-span, the method is satisfactory even for complex wing loadings. For most configurations, this covers the area of interest. If results beyond that point are required, some improvements in the technique are required.

This method should be incorporated in potential flow programs for the following reasons:

1) It provides an improved estimate of the angle for the Kutta condition application at the trailing edge. There, instead of using the trailing edge bisector slope, the total velocity vector direction should be used. One cycle should be efficient for this purpose.

2) It provides a rational evaluation method for stability derivatives and load conditions for trailing surfaces.

3) It can be easily incorporated in a potential flow method using parametric bicubic patches for source panels as well. Designers and analysts using these for geometric definition would find their effort to obtain the panel model greatly reduced.

Acknowledgments

The authors wish to acknowledge the partial support by the NASA-Ames Research Center and the Wichita State University and the assistance of Mr. Bijan Rashidian, a graduate student at WSU, for his help in implementing the curve shape improvement routines.

References

[1]Iversen, J. D., Park, S., Backhus, D. R., Brinkman, R. A., and Corsiglia, V. R., "Hot-Wire, Laser Anemometer and Force Balance Measurements in Cross-Sectional Planes of Single and Interacting Trailing Vortices," *Journal of Aircraft*, Vol. 16, 1979, pp. 448–456.

[2]Rossow, V. J., "Survey of Computational Methods for Lift Generated Wakes," NASA SP-347, March 1975.

[3]Rossow, V. J., "Inviscid Modeling of Aircraft Trailing Vortices," NASA SP-409, Feb. 1976.

[4]Hess, J. L. and Smith, A.M.O., "Calculation of Non-Lifting Potential Flow about Arbitrary Three-Dimensional Bodies," *Journal of Ship Research*, Vol. 8, Sept. 1964, pp. 22–42.

[5]Hess, J. L., "Calculation of Potential Flow about Arbitrary Three-Dimensional Lifting Bodies," MDC J5679-01, McDonnell-Douglas Co., Oct. 1972.

[6]Rubbert, P. E., "Theoretical Characteristics of Arbitrary Wings by a Nonplanar Vortex Lattice Method," D6-9244, The Boeing Co., 1964.

[7]Johnson, F. T. and Rubbert, P. E., "Advanced Panel-Type Influence Coefficient Methods Applied to Subsonic Flows," AIAA Paper 75-50, Jan. 1975.

[8]Hess, J. L., "A Higher Order Panel Method for Three-Dimensional Potential Flow," NADC 77166-30, June 1979.

[9]Hess, J. L. and Friedman, D. M., "An Improved Higher Order Panel Method for Three-Dimensional Lifting Potential Flow," NADC 79277-60, Dec. 1981.

[10]El-Ramly, Z., "Aircraft Trailing Vortices—A Survey of the Problem," ME/A 72-1, Faculty of Engineering, Division of Aerothermodynamics, Carleton Universtiy, Ottawa, Canada, Nov. 1972.

[11]Westwater, F. L., "The Rolling Up of the Surface Discontinuity Behind an Aerofoil of Finite Span," British Aeronautical Research Council, Reports and Memoranda 1692, 1935.

[12]Butter, D. J. and Hancock, G. J., "A Numerical Method for Calculating the Trailing Vortex System Behind a Swept Wing at Low Speed," *The Aeronautical Journal*, Vol. 75, Aug. 1971, pp. 564-568.
[13]Maskew, B., "Subvortex Techniques for the Close Approach to a Discretized Vortex Sheet," *Journal of Aircraft*, Vol. 14, Feb. 1977, pp. 188-193.
[14]Yeh, D. T. and Plotkin, A., "Vortex Panel Calculation of Wake Rollup Behind a Large Aspect Ratio Wing," AIAA Paper 85-1561, July 1985.
[15]Ferguson, J. C., "Multivariable Curve Interpolation," *J. ACM*, Vol. 11, 1964, pp. 221-228.
[16]Sikavi, D. A., "An Experimental and Theoretical Comparative Study of Boeing's Wake Turbulence Assessment System," D6-46383TN, The Boeing Co., July 1978.
[17]Betz, A., "Verhalten von Wirbelsystemen," *Zeitschrift fur Angewandte Mathematik und Mechanik*, Vol. 12, June 1932, pp. 164-174 (see also NACA TM713).